PAPER

Demonstration of Chaos-Based Radio Encryption Modulation Scheme through Wired Transmission Experiments

Kenya TOMITA[†a)], **Mamoru OKUMURA**[†], *Nonmembers, and* **Eiji OKAMOTO**[†], *Fellow*

SUMMARY With the recent commercialization of fifth-generation mobile communication systems (5G), wireless communications are being used in various fields. Accordingly, the number of situations in which sensitive information, such as personal data is handled in wireless communications is increasing, and so is the demand for confidentiality. To meet this demand, we proposed a chaos-based radio-encryption modulation that combines physical layer confidentiality and channel coding effects, and we have demonstrated its effectiveness through computer simulations. However, there are no demonstrations of performances using real signals. In this study, we constructed a transmission system using Universal Software Radio Peripheral, a type of software-defined radio, and its control software LabVIEW. We conducted wired transmission experiments for the practical use of radio-frequency encrypted modulation. The results showed that a gain of 0.45 dB at a bit error rate of 10^{-3} was obtained for binary phase-shift keying, which has the same transmission efficiency as the proposed method under an additive white Gaussian noise channel. Similarly, a gain of 10 dB was obtained under fading conditions. We also evaluated the security ability and demonstrated that chaos modulation has both information-theoretic security and computational security.

key words: *physical layer security, radio-wave encrypted modulation, software defined radio, chaos modulation*

1. Introduction

Recently, the commercialization of fifth-generation mobile communication systems (5G) has begun. By applying its characteristic requirements of ultra-high speed, high capacity, ultra-reliability, low latency, and massive simultaneous connections, 5G is expected to be used not only by wireless user terminals that have been targeted in long-term evolution (LTE) and fourth-generation mobile communication systems (4G), but also by automotive, industrial, home security, and other applications [1]. Accordingly, the demand for communication confidentiality is increasing in fields where important personal information is exchanged, such as in medical and financial fields [2]. Traditionally, security technologies such as SSL/TLS [3], which provide public key certificate-based authentication, secure session key establishment, and symmetric key-based traffic confidentiality, and IPSec [4], which provide integrity, confidentiality, and authentication of data communications over IP networks, have been used to meet these requirements. All of these technologies were performed using upper-layer protocols. Therefore, as communication infrastructures change with 5G evolution and networks become more complex in the future, security measures in the upper layers will need to adapt to increasingly complex networks. This result is likely to be a strong constraint for protocols and a high additional cost for the user. In addition, with the practical application of quantum computers, it is likely that cryptography based on computational security, such as Rivest-Shamir-Adleman (RSA), which is currently in use, will crack in the future [5].

Therefore, physical layer security (PLS) with information-theoretic security has attracted attention in recent years [6]–[8], focusing on the concealing ability of the propagation path. The first property of PLS is information-theoretic security, which ensures confidentiality regardless of the eavesdropper's computational ability. This enables secure and reliable communication without being deciphered, even when there is an eavesdropper with a sufficiently high computational power in the same network. Second, PLS can be applied in conjunction with existing upper-layer security technologies to enhance confidentiality because the physical layer operates independently, separate from the upper layers.

Several types of conventional PLSs have been proposed as follows:

(a) Directional modulation (DM) [9]:
The DM is a transmitter-side technique that sends an encoded signal in a pre-specified spatial direction and distorts the constellation of the same signal in other directions that are not specified. While a legitimate receiver can receive a normal signal, the eavesdropper receives a signal with a distorted constellation, making normal decoding difficult.

(b) Artificial noise (AN) [10]:
An AN is transmitted from the base station or is appended to the transmitted signal. This contaminates the received signal of the eavesdropper and therefore interferes with the normal decoding. Because an AN is based on a legitimate user channel, only a legitimate receiver can remove the AN.

(c) Radiofrequency fingerprinting (RFF) [11]
When a radio frequency (RF) signal is transmitted from a transmitter, the RF signal exhibits transient behavior with respect to the instantaneous frequency and amplitude. The behavior varies depending on various factors, including differences in the transmitted signal and the circuit configuration of the transmitter. The same transmitter may exhibit different behaviors depending on manufacturing tolerances and aging. This device-specific transient signal behavior is called RFF and is used to identify the transmitters. In

Manuscript received September 26, 2022.
Manuscript revised December 26, 2022.
Manuscript publicized January 25, 2023.

[†] The authors are with Department of Electrical and Mechanical Engineering, Graduate School of Engineering, Nagoya Institute of Technology, Nagoya-shi, 466-8555 Japan.
a) E-mail: ckl14087@nitech.jp

DOI: 10.1587/transcom.2022EBT0005

wireless networks, the identification of transmitters by RFF makes it possible to detect eavesdroppers with unknown RFF, thereby increasing security.
(d) Spread spectrum codes [12]:
Spread spectrum techniques, such as direct sequence spread spectrum (DSSS), have also attracted the attention of engineers because of their physical layer confidentiality. In DSSS, the spectrum of the transmitted signal is spread like white noise by a spreading code such as a pseudo-noise (PN) sequence. Therefore, the DSSS has many excellent characteristics, including jamming immunity and interference rejection. The spreading codes are not made public and are shared only between transmitters and receivers. This makes it difficult for an eavesdropper to despread the received signal, thereby enabling secure communication.

As one of the PLS technologies other than (a)–(d), we propose chaos modulation [13], which uses chaos randomness to ensure communication confidentiality. As this method uses first-order modulation, it can coexist with other PLS technologies and enhance security. In addition, unlike conventional PLS methods, chaos modulation has a channel-coding effect that enables high-quality communication. Because of such excellent characteristics of chaos modulation, we focused on using this PLS technology in our research. This scheme generates a chaos modulation signal using a Bernoulli shift map [14], which is a chaos generation formula to generate random signals, and a user-specific key signal based on a common-key cryptography scheme. As the key signal used in the modulation is shared between the sender and receiver, an eavesdropper who does not have the key cannot successfully demodulate the signal, thereby ensuring confidentiality.

The following method is proposed for chaos modulation enhancement. By replacing some of the chaos symbols with quadrature amplitude modulation (QAM) symbols, this method improves the transmission efficiency to 4 bit/symbol, which was previously 1 bit/symbol, and reduces the number of operations during demodulation [15]. Instead of using a Bernoulli shift map, a logistic map [16] was applied to increase the coding gain with the same number of operations [17]. In multi-user access schemes, chaos non-orthogonal multiple access (C-NOMA) [18], [19] has been considered. It applies chaos modulation to NOMA [20] that divides not only the frequency domain but also the power domain. A method to construct chaos interleave-division multiple access (IDMA) [21], [22] using chaos modulation and a chaos interleaver to achieve high system throughput has also been considered. Furthermore, synergistic improvement in transmission performance was achieved by externally concatenating powerful error-correcting codes such as polar codes and low-density parity-check (LDPC) codes [23], [24]. However, all of these studies were based on numerical simulations and have not been demonstrated with real signals.

On the other hand, [25]–[27] demonstrated transmission methods with physical layer confidentiality and conducted experiments on wireless communication using the characteristics of chaos signals. However, these existing studies have only demonstrated chaos spread-spectrum communication and not chaos communication that achieves coding gain instead of spreading gain. Moreover, similar to [25]–[27], there has been no comparison with linear modulation of the same transmission efficiency or an experimental investigation of the confidentiality of chaos.

Therefore, this study demonstrates the effects of previously proposed chaos modulation by conducting a wired transmission experiment using the universal software radio peripheral (USRP) N210 [28] and control software LabVIEW [29]. USRP N210 is a type of software-defined radio (SDR) [30], [31] that allows the implementation of a communication scheme by designing a computer program to process baseband signals. Our experiments show that a coding gain of 0.45 dB with a chaos block length of 10 at a bit error rate (BER) of 10^{-3} was obtained for binary phase-shift keying (BPSK) with the same transmission efficiency and that 10 dB gain was obtained with a chaos block length of 4 in a fading environment. We also experimentally evaluated the security and showed that chaos modulation has both information-theoretic and computational security.

The contributions of this study are as follows:
- First demonstration of the transmission of a chaos modulation signal with coding gain for BPSK.
- Demonstration of wired transmission of the proposed chaos modulation scheme using a software radio system that is close to an actual communication system.
- An experiment conducted to evaluate the confidentiality of chaos modulation and demonstrated that it is secure.

Section 2 describes the chaos modulation used in this study, and Sect. 3 describes the experimental setup. Section 4 presents the experimental results and discussion, and Sect. 5 provides a summary.

2. Chaos Modulation Composition

Figure 1 shows a block diagram of the chaos modulation. Chaos modulation uses block transmission, in which N_c symbols transmitted at a certain time are grouped together to form a single block [13]; where N_c is the chaos block length. First, we define a key signal $c_0 \in \mathrm{C}$ that is shared between the transmitter and receiver as follows:

$$0 < \mathrm{Re}\,[c_0] < 1, \quad 0 < \mathrm{Im}\,[c_0] < 1. \tag{1}$$

In this study, we assume that the key signal is shared between the transmitter and receiver in advance. The data sequence $\mathbf{b}$ of one chaos block is expressed as follows:

$$\mathbf{b} = [b_0, b_1, \cdots b_{N_c-1}] \in \{0, 1\}^{N_c}\,. \tag{2}$$

These c_0 and $\mathbf{b}$ are convolved according to Eq. (3), and the

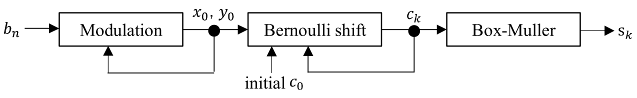

Fig. 1 Block diagram of chaos modulation.

initial values $x_0, y_0 \in \mathbb{R}$ for chaos processing are assigned to the chaos generation equation in Eq. (4).

$$x_0 = \begin{cases} \mathrm{Re}[c_{k-1}]\,(b_{k-1}=0) \\ 1-\mathrm{Re}\,[c_{k-1}]\left(b_{k-1}=1, \mathrm{Re}\,[c_{k-1}] > \dfrac{1}{2}\right) \\ \mathrm{Re}\,[c_{k-1}] + \dfrac{1}{2}\left(b_{k-1}=1, \mathrm{Re}\,[c_{k-1}] \le \dfrac{1}{2}\right) \end{cases},$$

$$y_0 = \begin{cases} \mathrm{Im}\,[c_{k-1}]\,(b_{k \bmod N_\mathrm{c}}=0), \\ 1-\mathrm{Im}\,[c_{k-1}]\left(b_{k \bmod N_\mathrm{c}}=1, \mathrm{Im}\,[c_{k-1}] > \dfrac{1}{2}\right) \\ \mathrm{Im}\,[c_{k-1}] + \dfrac{1}{2}\left(b_{k \bmod N_\mathrm{c}}=1, \mathrm{Im}\,[c_{k-1}] \le \dfrac{1}{2}\right) \end{cases}, \tag{3}$$

where $c_k \in \mathbb{C}$ is the $k(1 \le k \le N_\mathrm{c})$-th chaos symbol, and the key signal c_0 is used when $k = 1$. The calculated initial values are then substituted into the Bernoulli shift map in the following equation and repeated:

$$x_{l+1} = \begin{cases} 2x_l & (0 \le x_l < 0.5) \\ 2x_l - 1 & (0.5 \le x_l < 1) \end{cases}, \tag{4}$$

where $l \in \mathbb{N}$ denotes the number of chaotic iterations. This generates a chaos signal. The c_k value after the iterations is set as follows:

$$\begin{aligned} \mathrm{Re}\,[c_k] &= x_{[I+b_{(k-1+N_\mathrm{c}/2) \bmod N_\mathrm{c}}]}, \\ \mathrm{Im}\,[c_k] &= x_{[I+b_{(k-1+N_\mathrm{c}/2+1) \bmod N_\mathrm{c}}]}. \end{aligned} \tag{5}$$

where I is a fixed number of chaos processing iterations and $I = 60$ is used in this study, which guarantees the randomness of the chaos signal as shown in Appendix A. Thus, x_0 and y_0 correspond to the real and imaginary parts of the chaos initial-value signal for calculating c_k, respectively. Next, the obtained c_k is substituted into the following equation to obtain uniformly distributed signals $c_\mathrm{x}^{(k)}, c_\mathrm{y}^{(k)} \in \mathbb{R}$.

$$\begin{aligned} c_\mathrm{x}^{(k)} &= \frac{1}{\pi}\cos^{-1}\left[\cos\left\{37\pi\left(\mathrm{Re}\,[c_k] + \mathrm{Im}\,[c_k]\right)\right\}\right], \\ c_\mathrm{y}^{(k)} &= \frac{1}{\pi}\sin^{-1}\left[\sin\left\{43\pi\left(\mathrm{Re}\,[c_k] - \mathrm{Im}\,[c_k]\right)\right\}\right] + \frac{1}{2}. \end{aligned} \tag{6}$$

Finally, by applying $c_\mathrm{x}^{(k)}, c_\mathrm{y}^{(k)}$ to the Box-Muller method [32], we can generate a chaos-based Gaussian-modulated transmitted signal $s(k) \in \mathbb{C}$ as follows:

$$s(k) = \sqrt{-\ln\left(c_\mathrm{x}^{(k)}\right)}\left\{\cos\left(2\pi c_\mathrm{y}^{(k)}\right) + \mathrm{j}\sin\left(2\pi c_\mathrm{y}^{(k)}\right)\right\}. \tag{7}$$

Let $H(k) \in \mathbb{C}$ denote the propagation channel coefficients and $n(k) \in \mathbb{C}$ denote the thermal noise. Then, the received signal series $y(k) \in \mathbb{C}$ in the receiver is given by

$$y(k) = H(k)s(k) + n(k). \tag{8}$$

Next, we describe the decoding method used. Decoding is performed for each chaos block using maximum likelihood sequence estimation (MLSE) [33]. First, all possible candidate signal sequences $\hat{s}(k) \in \mathbb{C}$ are generated using c_0 shared with the transmitter. A replica signal sequence is also generated from $\hat{s}(k)$ and $H(k)$. Next, the sum of the squared Euclidean distances between the received signal series $y(k)$ and the replica signal series are calculated for all candidates. The candidate signal with the minimum sum of the distances is estimated as the transmit signal, and the corresponding bit sequence $\hat{\mathbf{b}} \in \{0, 1\}$ can be determined as the decoded result, which is given by

$$\hat{\mathbf{b}} = \underset{\mathbf{b}}{\mathrm{argmin}} \sum_{k=1}^{N_\mathrm{c}} |y(k) - H(k)\hat{s}(k)|^2. \tag{9}$$

See [13] for details on the modulation and demodulation schemes.

3. Experimental Methods and Signal Configuration

This section first describes the experimental system and transmitting frame format and then details the experimental method and signal processing in the receiver.

3.1 Structure of Software Defined Radio

We used software-defined radio that combined Ettus Research's USRP N210 with an XCVR2450 daughter board. The USRP series could be used with different frequency ranges and configurations, depending on the daughter boards to be combined. Tables 1 and 2 list the transmitter and receiver specifications, respectively [34], and Fig. 2 shows the block diagram of the USRP. At the transmitter, the USRP receives the transmitting baseband signals and control information from the control PC via Ethernet. Next, the sampled points of the baseband signal are pre-upconverted using a digital up converter (DUC) and then transformed from a digital signal to an analog signal using a digital-to-analog converter (DAC). The converted analog signal is passed through a low-pass filter (LPF), converted to RF signals by quadrature modulation, and amplified by the amplifier. Subsequently, it is transmitted from either TX1 or TX2 antenna terminals. The RF signals are received from

Table 1 Transmitter specifications.

Device	USRP N210+XCVR2450
Frequency range	2.4 GHz to 2.5 GHz 4.9 GHz to 6.0 GHz
Frequency step	<1 kHz
Maximum output power	50 mW to 100 mW (17 dBm to 20 dBm)
Gain range	0 dB to 35 dB
Gain step	0.5 dB
Maximum instantaneous real-time bandwidth	16 bit sample width: 24 MHz 8 bit sample width: 48 MHz
Digital-analog converter	2 channels, 400 MS / s, 16 bit
Maximum IQ sample rate	16 bit sample width: 25 MS / s 8 bit sample width: 50 MS / s
Interface	Gigabit Ethernet
Full duplex/Half duplex	Half duplex (2ch)

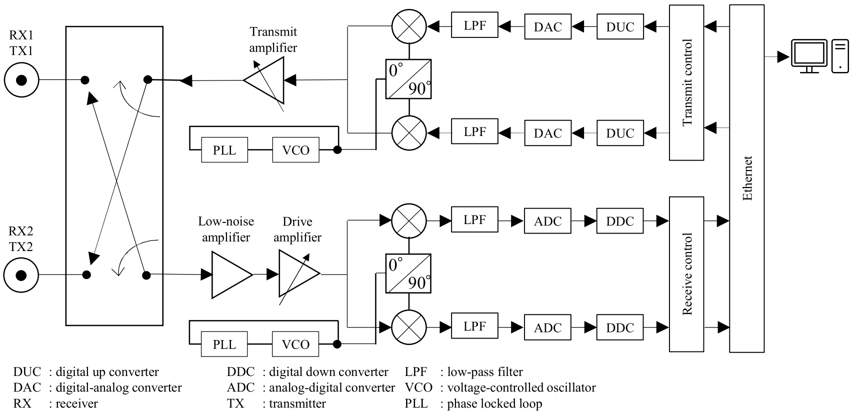

Fig. 2 Block diagram of USRP.

Table 2 Receiver specifications.

Device	USRP N210+XCVR2450
Frequency range	2.4 GHz to 2.5 GHz 4.9 GHz to 6.0 GHz
Frequency step	<1 kHz
Maximum input power	-15 dBm
Gain range	0 dB to 92.5 dB
Gain step	2 dB
Maximum instantaneous real-time bandwidth	16 bit sample width: 19 MHz 8 bit sample width: 36 MHz
Analog-digital converter	2 channels, 100 MS / s, 14 bit
Maximum IQ sample rate	16 bit sample width: 25 MS / s 8 bit sample width: 50 MS / s
Interface	Gigabit Ethernet
Full duplex/Half duplex	Half duplex (2ch)

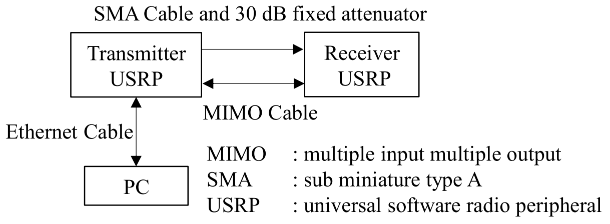
SMA Cable and 30 dB fixed attenuator
Transmitter USRP
Receiver USRP
MIMO Cable
Ethernet Cable
PC
MIMO : multiple input multiple output
SMA : sub miniature type A
USRP : universal software radio peripheral

Fig. 3 Block diagram of the experimental setup.

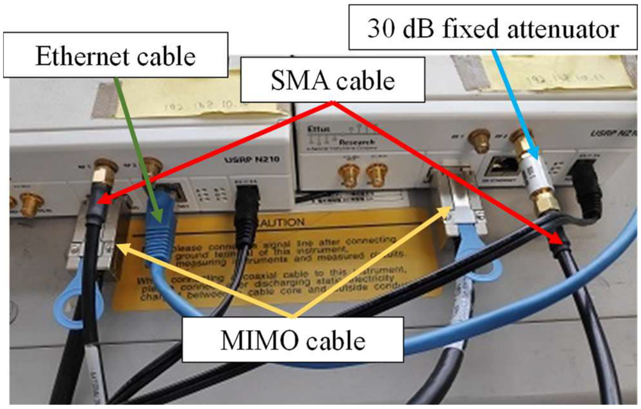

Fig. 4 Connection of experimental equipment.

either the RX1 or RX2 antenna terminals. The received RF signal is amplified by the amplifier and converted into a baseband signal by orthogonal demodulation. This is then passed through the LPF and converted from an analog signal to a digital signal by an analog-to-digital converter (ADC), and the sampled points are reduced by a digital down converter (DDC). Subsequently, the signal is sent to a PC via Ethernet.

3.2 Experimental Method

First, the experimental system is described. Figures 3 and 4 show a block diagram of the experimental setup and a photograph of the equipment connections, respectively. The transmitting and receiving USRPs are connected by a multiple-input multiple-output (MIMO) cable [35] and a subminiature type A (SMA) cable coupled with a 30 dB fixed attenuator [36]. The MIMO cable is used only for time and frequency synchronization between USRPs, that is, RF data is not transmitted via the MIMO cable. Instead of antennas, coaxial cables with SMA connectors are used to transmit RF signals. Here, only the transmitting USRP is connected to the PC with an Ethernet cable, because the USRPs are bridged by the MIMO cable. The control software on the PC is LabVIEW version 20.0f1. Figures 5 and 6 show the block diagrams of the signal transmission and framework of the transmitting signal, respectively. In the transmitter, 2,000 symbols of chaos modulation signals were generated for 500 subframes, according to the modulation scheme described in Sect. 2. Subsequently, 256 symbols of the preamble signal and 48 symbols of the pilot signal were generated and inserted. The compositions of these signals are described in the following subsections. Furthermore, to simulate fading environments in the experiment, fading signals were generated and multiplied by transmitted signals. As shown in Fig. 3, the composed frame was transmitted and received using the USRP via the SMA cable, and the PC received and stored the digital data of the received signal from the USRP receiver. Offline processing was used to perform frame synchronization and amplitude/phase correction, as described in Sect. 3.4, and MLSE was performed on each

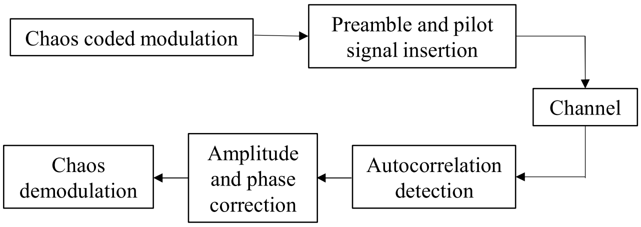
Chaos coded modulation
Preamble and pilot signal insertion
Channel
Autocorrelation detection
Amplitude and phase correction
Chaos demodulation

Fig. 5 Block diagram of signal transmission.

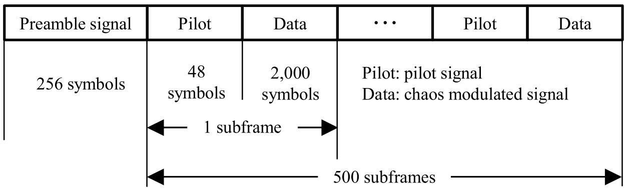

Fig. 6 Framework of transmit signal.

received chaos modulation block for demodulation.

3.3 Preamble Signal Composition and Frame Synchronization Method

In this study, the 256 preamble symbols were composed of 255 symbols of degree 8 M-sequence [37], calculated using the following primitive polynomial $f(x)$ for a finite variable x and one zero symbol.

$$f(x) = x^8 + x^4 + x^3 + x^2 + 1. \tag{10}$$

At the receiver side, the cross-correlation [38] between the preamble signal and the received signal is calculated as follows:

$$A_i = \sum_{k=0}^{255} \mathrm{Re}\left[p_k\right] \mathrm{Re}\left[r_{k+i}\right] + \mathrm{Im}\left[p_k\right] \mathrm{Im}\left[r_{k+i}\right], \tag{11}$$

where $r_{k+i} \in \mathbb{C}$ $(0 \le k \le 255, i \in \mathbb{Z})$, $p_k \in \mathbb{C}$, and $A_i \in \mathbb{R}$ are the $(k+i)$-th received signal, k-th preamble signal, and i-th cross-correlation value, respectively. The highest correlation point with the maximum A_i value can be determined as the starting point of the preamble in the received signal, thereby allowing frame synchronization. The cross-correlation values at the frame synchronization point are sharp and pulse-like, preventing misinterpretation.

3.4 Receiver-Side Equalization Process Using Pilot Signals

In the experiments, various factors caused amplitude and phase distortions in the received signals. Pilot signal transmission was used to compensate for this. First, the average phase value θ_{avg} [rad] of the phase difference of the pilot signals between the transmitter and receiver was calculated as follows, and the phase of the following 2,000 chaos symbols was rotated by $-\theta_{\mathrm{avg}}$ to correct the phase distortion.

$$\theta_{\mathrm{avg}} = \frac{1}{M} \sum_{i=0}^{M-1} \left\{\theta_{\mathrm{pilot},i} - \varphi_{\mathrm{TX},i}\right\}. \tag{12}$$

Here, $M(=48)$, $\theta_{\mathrm{pilot},i}$, and $\varphi_{\mathrm{TX},i}$ are the number of pilot symbols in one subframe, the phase of the i-th received signal of the pilots, and the phase of the i-th transmitted signal, respectively. In this study, BPSK signals were used as pilot signals because they have a constant amplitude at the sampling point, a low peak-to-average power ratio (PAPR), and low nonlinear distortion when passed through a power amplifier. Therefore, the transmission channel characteristics could be accurately estimated [39]. Next, to correct the amplitude of the received signal, the following equation was used on the receiver side:

$$|\hat{r}_i| = |r_i| \sqrt{\frac{P_{\mathrm{t}}}{P_{\mathrm{r}} - P_{\mathrm{noise}}}}, \tag{13}$$

where $\hat{r}_i \in \mathbb{C}$, P_{t}, P_{r}, and P_{noise} are the compensated received chaos signals, average transmitting power at the pilots, average received signal power at the pilots, and average received noise power, respectively. Here, P_{noise} is measured when null signals with zero amplitude are transmitted in advance. The amplitude correction ratio between the transmitted and received signals can be calculated using the square root of the power, and thus the equalization can be conducted by (13).

4. Experimental Results and Performance Evaluation

First, the frame synchronization, amplitude, and phase correction performances were examined. Then, the BER characteristics of chaos modulation under additive white Gaussian noise (AWGN) and fading environments were measured to demonstrate that the channel coding effect was obtained. Finally, the information theory and computational security of chaos modulation were evaluated experimentally.

4.1 Synchronization and Equalization Performance

We evaluated the performance of the frame synchronization, amplitude, and phase correction using the methods described in Sect. 3. To obtain the pure characteristics of the signal variations generated by the experimental equipment, the experiments were conducted in an AWGN environment, where propagation channel variations are not necessarily considered. The experimental conditions are listed in Table 3. The cross-correlation function of the received signal was measured when the average signal-to-noise ratio (SNR) was 0 dB. The results in Fig. 7 show that a pulse-like value can be found at a certain synchronization point near the 5,000 symbol index on the horizontal axis.

This confirms that frame synchronization is achieved at 0 dB. Because the experiments in this study were performed at an average received SNR greater than 0 dB, we can conclude that the frame synchronization performance was sufficient.

Table 3 Experimental conditions under AWGN environment.

Center frequency	5.015 GHz
IQ rate	4 MS/s
Receiver gain	[0, 30] dB
Transmitter gain	[0, 30] dB
Data length	10^6 bit
No. of samples per symbol	4
Chaos block length N_c	10
No. of chaos processing iterations	60
Channel model	AWGN

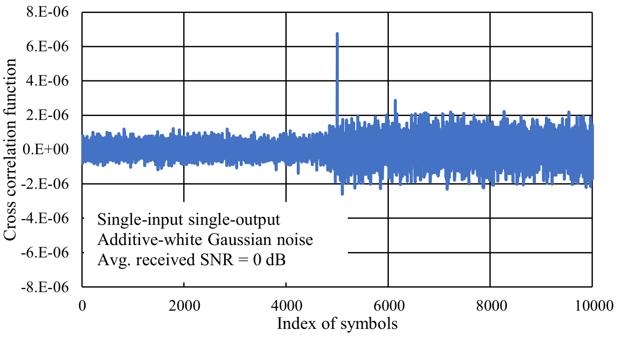

Fig. 7 Cross-correlation value between pilot and received signals when average received SNR = 0 dB.

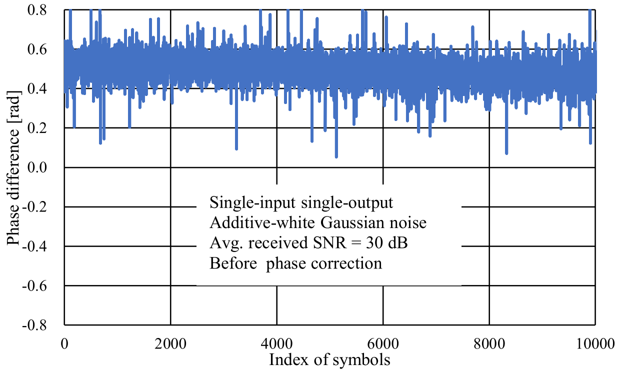

Fig. 8 Phase difference before correction when average received SNR = 30 dB.

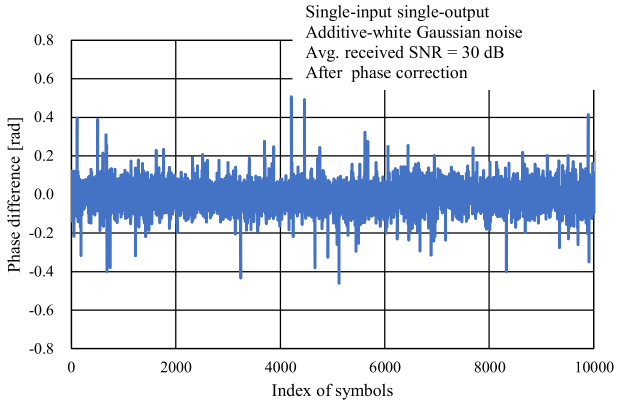

Fig. 9 Phase difference after correction when average received SNR = 30 dB.

Next, the phase correction by the pilot signals was evaluated under the same conditions as those in Table 3. The phase difference between the transmitted and received signals was measured at an average received SNR of 30 dB to suppress the channel noise and evaluate the behavior of the experimental equipment. Figures 8 and 9 show the phase differences before and after correction versus the symbol index, respectively. These figures show that the fixed offset was removed by phase correction; however, the random phase differences remained uncorrected. This is because there are two sources of phase differences generated during transmission in USRPs. The phase difference $\theta_{\mathrm{offset},i}$ between the transmitted and received signals at the i-th symbol can be expressed as follows [40]:

$$\theta_{\mathrm{offset},i} = \theta_{\mathrm{CORDIC}} + \theta_{\mathrm{PLL},i}, \tag{14}$$

where θ_{CORDIC} denotes the fixed phase difference generated by the USRP coordinate rotation digital calculation (CORDIC) algorithm. The CORDIC algorithm is a vector rotation method at arbitrary angles using shifts and adders, as presented by Volder in 1959. This allows the computation of sine, cosine, magnitude, and phase trigonometric functions with arbitrary precision [41]. However, the starting position of the CORDIC in the USRP is randomly determined at power-on; therefore, a random offset is generated every time the channel is initialized. Also, it does not change during the operation and remains constant, allowing for correction by pilot signals. On the other hand, $\theta_{\mathrm{PLL},i}$ is caused by ambiguity in the phase-locked loop (PLL) circuit inside the USRP. In USRP, a 10 MHz reference clock generated by a local oscillator (LO) is converted to a frequency signal used for quadrature conversion by a voltage-controlled oscillator (VCO) and a PLL circuit. In this study, the 10 MHz reference clock is shared by the MIMO cable, and there is no phase shift caused by the LO. Because the VCO and PLL circuits are not shared, ambiguities in the PLL circuits cause fluctuations in the phase of the frequency signal at each USRP, and the phases of the transmitted and received signals change with $\theta_{\mathrm{PLL},i}$ [42]. Although $\theta_{\mathrm{PLL},i}$ is a random value that is difficult to compensate for by piloting, its effect on the transmission characteristics is negligible owing to its small value.

Finally, transmission experiments were conducted under the same conditions as those listed in Table 3. The waveforms of the transmitted and equalized chaos signals in the transmitter and receiver, respectively, are shown in Fig. 10 at an average received SNR of 30 dB. The results show that the transmitted and received signals are consistent, indicating that the amplitude and phase corrections worked appropriately.

4.2 Transmission Characteristics in AWGN Environment

Transmission experiments to measure the BER characteristics of the chaos modulation were conducted under the same conditions as those in Table 3. For comparison, the performances of the BPSK with equal transmission efficiencies

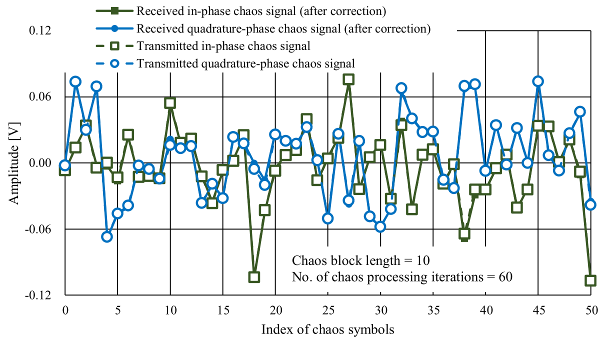

Fig. 10 Chaos modulation signal after equalization.

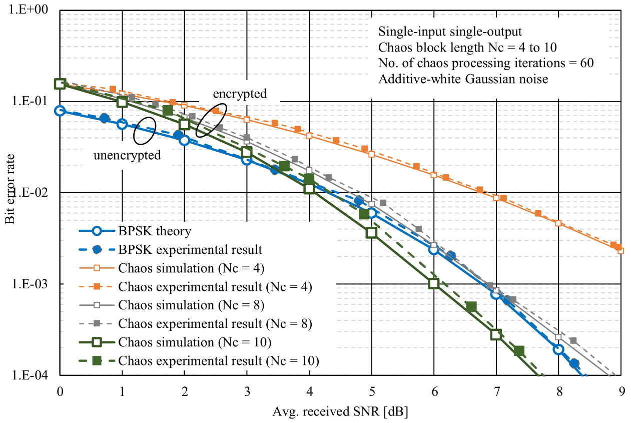

Fig. 11 Experimental results of BER characteristics in AWGN environment.

were compared. In this study, user-specific keys c_0 used in chaos modulation were randomly generated for each transmission, and these keys were shared in advance. Figure 11 shows the results, where the performance of chaos modulation is gradually improved as the chaos block length N_c increases because the chaos channel coding gain increases. When $N_c = 10$, the performance of chaos modulation is superior to that of BPSK, with a gain of 0.45 dB at a BER of 10^{-3}. This demonstrates that the coding gain of the chaos modulation can be obtained in real environments.

4.3 Transmission Characteristics in Fading Environment

Next, the chaos block length N_c was set to 4, the other conditions were the same as those in Table 3, and the experiments were conducted in a fading environment. By multiplying the transmitted signal by the fading signal, the channel is assumed to be symbol-to-symbol independent, identically distributed quasi-static Rayleigh fading. The channel information on the receiver side is assumed to be perfectly known. The results illustrated in Fig. 12 show that chaos modulation provides a gain of 10 dB at a BER of 10^{-3} compared with BPSK. This confirms that the coding gain of chaos modulation can be obtained in a fading environment as well as in an AWGN. In addition, because of the channel-diversity effect, the coding gain is obtained with a shorter block length of $N_c = 4$.

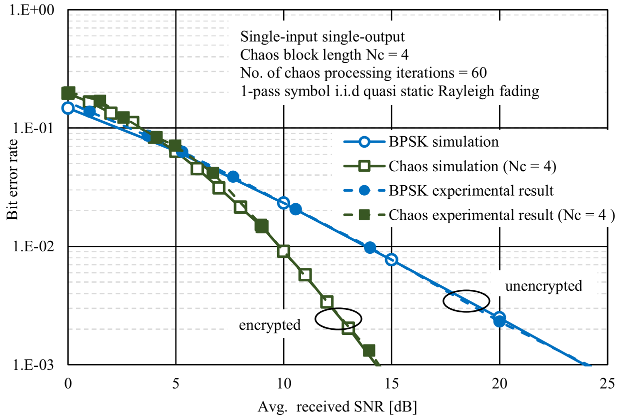

Fig. 12 Experimental results of BER characteristics in fading environment.

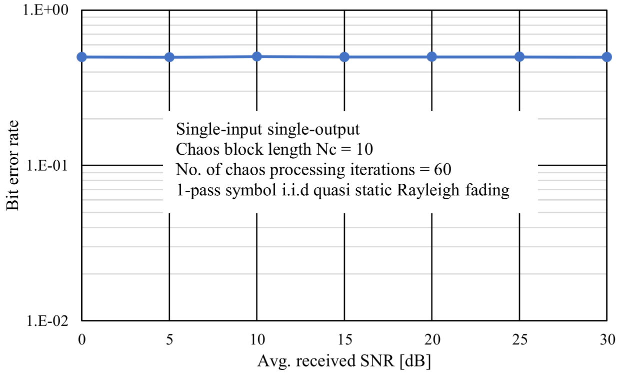

Fig. 13 BER characteristics of eavesdroppers.

4.4 Security Evaluation

The security of the chaos modulation was verified experimentally. Security against eavesdroppers is generally evaluated from two perspectives: information theory and computational security. Information-theoretic security is evaluated based on Shannon's theory of cryptography [43], where the characteristics of the environment of the eavesdropper are changed and a decoding trial is conducted. Computational security, on the other hand, is evaluated in terms of the number of operations 2^m required to decrypt the code using the optimal algorithm. This cipher is then said to be computationally secure with $m \in \mathbb{R}$ bits security [44]. Because the modulated chaos signal depends on the user-specific key signal, a full-key search is the optimal method for decryption.

Experiments were conducted under the same conditions as in Sect. 4.3, and the BER of the eavesdropper, in which the key signal was randomly generated to evaluate the information-theoretic security, is shown in Fig. 13. To emphasize the eavesdropping effect, a strong channel coding gain of $N_c = 10$ was used. The wiretap channel was simulated using the same received signals as Bob but using

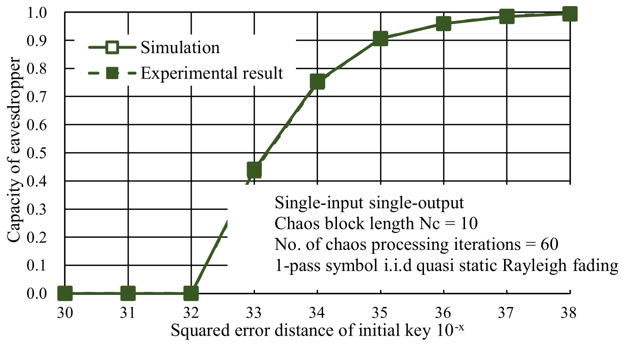

Fig. 14 Channel capacity characteristics of eavesdroppers.

Eve's key. Furthermore, to measure the computational security, the eavesdropper's channel capacity C_R was calculated as the squared Euclidean distance between the key probed by the eavesdropper and the legitimate key. C_R can be obtained from BER of the eavesdropper P_e [45] as follows:

$$C_R = 1 + P_e \log_2 P_e + (1 - P_e) \log_2(1 - P_e). \qquad (15)$$

The results are shown in Fig. 14. As it has already been confirmed in computer simulations that chaos modulation has both information-theoretic and computational securities [15], [46], in this wired transmission experiment, the results shown in Figs. 13 and 14 support the results of those literatures. Specifically, Fig. 13 shows that the BER is constant at 0.5, regardless of the average received SNR. Fig. 14 shows that the eavesdropper's channel capacity is zero at key distances of 10^{-32} or less, which is equivalent to $m = 64$. Thus, the same security as in [15] and [46] has been demonstrated for real signal transmission.

5. Conclusion

In this study, we conducted wired transmission experiments on chaos modulation using software-defined radios, measured BER characteristics under AWGN and fading environments, and confirmed that coding gains were obtained. We also conducted experiments on security, showing that chaos modulation has excellent properties in terms of both information-theoretic and computational securities. This shows that chaos modulation, which has not been demonstrated previously, is effective even in a wired environment.

Acknowledgments

We thank Mr. Yuki Mori of our laboratory for his experimental support. This study was supported by JSPS KAKENHI (grant number 22K04102).

References

[1] A. Osseiran, F. Boccardi, V. Braun, K. Kusume, P. Marsch, M. Maternia, O. Queseth, M. Schellmann, H. Schotten, H. Taoka, H. Tullberg, M.A. Uusitalo, B. Timus, and M. Fallgren, "Scenarios for 5G mobile and wireless communications: The vision of the METIS project," IEEE Commun. Mag., vol.52, no.5, pp.26–35, May 2014.

[2] I. Ahmad, T. Kumar, M. Liyanage, J. Okwuibe, M. Ylianttila, and A. Gurtov, "Overview of 5G security challenges and solutions," IEEE Commun. Stand. Mag., vol.2, no.1, pp.36–43, March 2018.

[3] C. Brubaker, S. Jana, B. Ray, S. Khurshid, and V. Shmatikov, "Using Frankencerts for automated adversarial testing of certificate validation in SSL/TLS implementations," 2014 IEEE Symposium on Security and Privacy, pp.114–129, Nov. 2014.

[4] Cisco Systems, "Configuring IPSec network security," Cisco IOS Security Configuration Guide, Release 12, 2, 2003.

[5] V. Bhatia and K.R. Ramkumar, "An efficient quantum computing technique for cracking RSA using Shor's algorithm," 2020 IEEE 5th International Conference on Computing Communication and Automation (ICCCA), pp.89–94, Oct. 2020.

[6] Y. Liu and H. Chen, "Physical layer security for next generation wireless networks: Theories, technologies, and challenges," IEEE Commun. Surveys Tuts., vol.19, no.1, pp.347–376, Aug. 2016.

[7] Y. Wu, A. Khisti, C. Xiao, G. Caire, K.K. Wong, and X. Gao, "A survey of physical layer security techniques for 5G wireless networks and challenges ahead," IEEE J. Sel. Areas Commun., vol.36, no.4, pp.679–695, April 2018.

[8] A. Mukherjee, S.A.A. Fakoorian, J. Huang, and A.L. Swindlehurst, "Principles of physical layer security in multiuser wireless networks: A survey," IEEE Commun. Surveys Tuts., vol.16, no.3, pp.1550–1573, Feb. 2014.

[9] Q. Cheng, V. Fusco, J. Zhu, S. Wang, and F. Wang, "WFRFT-aided power-efficient multi-beam directional modulation schemes based on frequency diverse array," IEEE Trans. Wireless Commun., vol.18, no.11, pp.5211–5226, Nov. 2019.

[10] S. Liu, Y. Hong, and E. Viterbo, "Practical secrecy using artificial noise," IEEE Commun. Lett., vol.17, no.7, pp.1483–1486, July 2013.

[11] O. Ureten and N. Serinken, "Wireless security through RF fingerprinting," Can. J. Electr. Comput. Eng., vol.32, no.1, pp.27–33, May 2007.

[12] T. Kang, X. Li, C. Yu, and J. Kim, "A survey of security mechanisms with direct sequence spread spectrum signals," Journal of Computing Science and Engineering, vol.7, no.3, pp.187–197, Sept. 2013.

[13] E. Okamoto, "A chaos MIMO transmission scheme for channel coding and physical-layer security," IEICE Trans. Commun., vol.E95-B, no.4, pp.1384–1392, April 2012.

[14] P.C. Shields, The Theory of Bernoulli Shift, University of Chicago Press, May 2009.

[15] T. Kaga, M. Okumura, E. Okamoto, and T. Yamamoto, "Multi-level encrypted transmission scheme using hybrid chaos and linear modulation," IEICE Trans. Commun., vol.E105-B, no.5, pp.638–647, May 2022.

[16] L. Kocarev, J. Szczepanski, J.M. Amigo, and I. Tomovski, "Discrete chaos-I: Theory," IEEE Trans. Circuits Syst. I, Reg. Papers, vol.53, no.6, pp.1300–1309, June 2006.

[17] M. Okumura, T. Kaga, E. Okamoto, and T. Yamamoto, "Improvement of channel coding gain of chaos modulation using logistic maps," IEICE Commun. Express, vol.10, no.9, pp.744–750, Sept. 2021.

[18] N. Horiike, E. Okamoto, and T. Yamamoto, "A downlink non-orthogonal multiple access scheme having physical layer security," J. Wireless Com. Networking, vol.2018, no.1, pp.1–11, Aug. 2018.

[19] E. Okamoto, "Overview of nonlinear signal processing in 5G and 6G access technologies," Nonlinear Theory and Its Applications, IEICE, vol.E12-N, no.3, pp.1–18, July 2021.

[20] Y. Saito, Y. Kishiyama, A. Benjebbour, T. Nakamura, A. Li, and K. Higuchi, "Non-orthogonal multiple access (NOMA) for cellular future radio access," 2013 IEEE 77th Vehicular Technology Conference (VTC Spring), pp.1–5, 2013.

[21] M. Okumura, E. Okamoto, Y. Masuda, T. Kaga, and T. Yamamoto, "Application of radio-wave encryption to interleave-division multiple-access scheme," Proc. International Symposium on Nonlinear Theory and its Applications (NOLTA 2020), pp.350–

353, Nov. 2020.

[22] M. Okumura, T. Kaga, E. Okamoto, and T. Yamamoto, "Chaos-based interleave division multiple access scheme with physical layer security," IEEE 18th Annual Consumer Communications & Networking Conference (CCNC), pp.1–2, 2021.

[23] N. Horiike, E. Okamoto, and T. Yamamoto, "Performance improvement of chaos MIMO transmission scheme by LDPC code concatenation using symbol MAP detection and STBC," Proc. Int'l Conf. on Information Networking (ICOIN2017), pp.200–205, Jan. 2017.

[24] K. Asano, M. Okumura, T. Abe, E. Okamoto, and T. Yamamoto, "High-quality secure wireless transmission scheme using polar codes and radio-wave encrypted modulation," IEICE Trans. Commun., vol.E106-B, no.4, pp.374–383, April 2023.

[25] C. Bai, H.-P. Ren, and C. Grebogi, "Experimental phase separation differential chaos shift keying wireless communication based on matched filter," IEEE Access, vol.7, pp.25274–25287, Feb. 2019.

[26] H.-P. Ren, C. Bai, J. Liu, M.S. Baptista, and C. Grebogi, "Experimental validation of wireless communication with chaos," Chaos: An Interdisciplinary Journal of Nonlinear Science, vol.26, no.8, pp.1–9, Aug. 2016.

[27] A.S. Dmitriev, A.V. Kletsov, A.M. Laktyushkin, A.I. Panas, and S.O. Starkov, "Ultrawideband wireless communications based on dynamic chaos," J. Commun. Technol. Electron., vol.51, pp.1126–1140, Oct. 2006.

[28] Ettus Research, "N200/N210," [Online] Available: https://kb.ettus.com/N200/N210

[29] National Instruments, "Labview," [Online] Available: https://www.ni.com/ja-jp/shop/labview.html

[30] T. Ulversøy, "Software defined radio: Challenges and opportunities," IEEE Commun. Surveys Tuts., vol.12, no.4, pp.531–550, May 2010.

[31] A.L. Garcia Reis, A.F. Barros, K. Gusso Lenzi, L.G. Pedroso Meloni, and S.E. Barbin, "Introduction to the software-defined radio approach," IEEE Latin America Transactions, vol.10, no.1, pp.1156–1161, Jan. 2012.

[32] G. Box and M. Muller, "A note on the generation of random normal deviates," Ann. Math. Statist., vol.29, no.2, pp.610–611, 1958.

[33] R. Raheli, A. Polydoros, and C. Tzou, "Per-Survivor processing: A general approach to MLSE in uncertain environments," IEEE Trans. Commun., vol.43, no.2/3/4, pp.354–364, Feb./Mar./April 1995.

[34] National Instruments, "USRP-2921 Specifications," [Online] Available: https://www.ni.com/documentation/en/usrp-software-defined-radio-device/latest/specs-usrp-2921/specs

[35] Ettus Research, "Synchronization and MIMO Capability with USRP Devices," [Online] Available: https://kb.ettus.com/Synchronization_and_MIMO_Capability_with_USRP_Devices

[36] Ettus Research, "Loop Back Cable Kit," [Online] Available: https://www.ettus.com/all-products/lpbk-kit

[37] Z. Xinyu, "Analysis of M-sequence and Gold-sequence in CDMA system," IEEE 3rd International Conference on Communication Software and Networks, pp.466–468, 2011.

[38] A. Fort, J. Weijers, V. Derudder, W. Eberle, and A. Bourdoux, "A performance and complexity comparison of auto-correlation and cross-correlation for OFDM burst synchronization," 2003 IEEE International Conference on Acoustics, Speech, and Signal Processing, 2003. Proceedings. (ICASSP'03), pp.341–344, April 2003.

[39] C.D. Moffatt and J. Hoffmann, "Low PAPR preamble for improved channel estimation," MILCOM 2008 - 2008 IEEE Military Communications Conference, pp.1–7, Nov. 2008.

[40] J.E. Volder, "The CORDIC trigonometric computing technique," IRE Trans. Electron. Comput., vol.EC-8, no.3, pp.330–334, Sept. 1959.

[41] J.R. Van der Merwe, J. Malan, F.D.V. Maasdorp and W.P. Du Plessis, "Multi-channel software defined radio experimental evaluation and analysis," Proc. Instituto Tecnologico de Aeronautica (ITA), 2014.

[42] S. Corum, J.D. Bonior, R.C. Qiu, N. Guo, and Z. Hu, "Evaluation of phase error in a software-defined radio network testbed," 2012 Proc. IEEE Southeastcon, pp.1–4, March 2012.

[43] C.E. Shannon, "Communication theory of secrecy systems," Bell Syst. Tech. J., vol.28, no.4, pp.656–715, Oct. 1949.

[44] Q. Dang, "Recommendation for Applications Using Approved Hash Algorism," NIST Special Publication 800-107, pp.1–22, Aug. 2012.

[45] A.J. Goldsmith and P.P. Varaiya, "Capacity, mutual information, and coding for finite-state Markov channels," IEEE Trans. Inf. Theory, vol.42, no.3, pp.868–886, May 1996.

[46] M. Okumura, K. Asano, T. Abe, E. Okamoto, and T. Yamamoto, "Performance improvement of radio-wave encrypted MIMO communications using average LLR clipping," IEICE Trans. Commun., vol.E105-B, no.8, pp.931–943, Aug. 2022.

Appendix: Consideration of Chaos Processing Iterations

We verified that the number of chaos processing iterations, I, which guarantees the randomness of the chaos signal, is greater than or equal to 60. We input slightly different initial values, x_0 and x'_0, to Eq. (4), ran the equation I times, and calculated the difference between the output values, x_I and x'_I. The difference from the normal key was set as the smallest case of 10^{-16} that can be expressed using the computational resolution of the C language. One million initial values were randomly generated, and the average value was calculated. The results are shown in Fig. A· 1, where it can be observed that the signal difference reaches a maximum when the number of chaos-processing iterations is greater than 60. This means that if the iteration number is greater than 60, the key generates a different chaos signal even when the initial key is close at a distance of 10^{-16}, thus maintaining security.

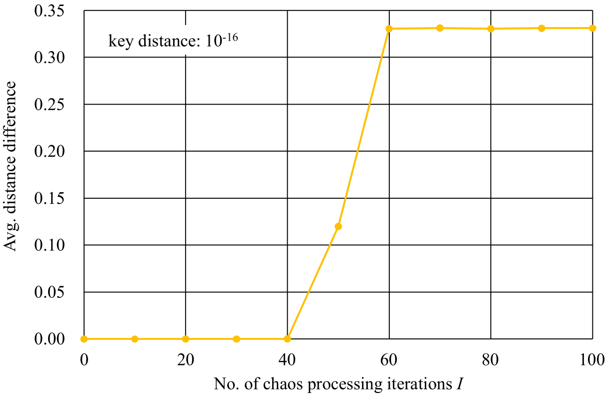

Fig. A· 1 Average distance characteristics of generated signal versus number of chaos processing iterations I.

Kenya Tomita received the B.E. and M.S. degrees in Electrical and Mechanical Engineering from Nagoya Institute of Technology in 2020 and 2022, respectively. His research interests are in the area of wireless communication technologies and their experiments, including chaos modulation.

Mamoru Okumura received the B.E. and M.S. degrees in Electrical and Mechanical Engineering from Nagoya Institute of Technology in 2020 and 2022, respectively. His research interests are in the area of wireless communication technologies, including physical layer security.

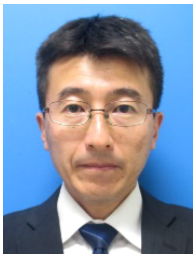

Eiji Okamoto received the B.E., M.S., and Ph.D. degrees in Electrical Engineering from Kyoto University in 1993, 1995, and 2003, respectively. In 1995 he joined the Communications Research Laboratory (CRL), Japan. Currently, he is an associate professor at Nagoya Institute of Technology. In 2004 he was a guest researcher at Simon Fraser University. He received the Young Researchers' Award in 1999 from IEICE and the FUNAI Information Technology Award for Young Researchers in 2008. His current research interests are in the areas of wireless technologies, mobile communication systems, wireless security, and satellite communications. He is a member of IEEE.